THE JOURNAL OF PHYSICAL CHEMISTRY C

Article

Cite This: J. Phys. Chem. C 2018, 122, 24164−24170

pubs.acs.org/JPCC

Acid-Promoted Crystallization of Amorphous Solid Water

Du Hyeong Lee and Heon Kang*

Department of Chemistry, Seoul National University, 1 Gwanak-ro, Seoul 08826, Republic of Korea

Supporting Information

ABSTRACT: In this study, the effect of externally added hydrogen chloride (HCl) on the crystallization of amorphous solid water (ASW) has been examined. ASW films containing small amounts of HCl, which dissociated into H^+ (excess protons) and Cl^- ions, and having a thickness of 90−360 monolayers (ML) were prepared on a Pt(111) substrate under an ultrahigh vacuum environment. The location of HCl in the samples was varied by controlling the stacking sequence of H_2O and HCl during the film growth. Crystallization kinetics of these samples were examined by conducting temperature-programmed desorption experiments and isothermal kinetic measurements with reflection−absorption infrared spectroscopy for the temperature range of 137−145 K. Crystallization behaviors of pure and NaCl-doped ASW films were also examined for comparison. The results indicated that the excess protons accelerated the crystallization of the ASW films, in contrast to the retardation effect of Na^+. In the presence of 0.1 ML HCl, the overall activation energy of ASW crystallization was reduced from 63.4 kJ·mol^{-1} in the absence of HCl to 48.5 kJ·mol^{-1}, which is close to the activation energy of crystal growth. The crystallization started near the location of HCl injection in the samples, regardless of whether it was the vacuum/ASW interface or the film interior. These observations indicated that the excess protons facilitated the nucleation process and changed the rate-limiting step of ASW crystallization from nucleation to growth. An explanation based on thermodynamics has been proposed, that is, the configurational entropy of the excess protons in ice likely reduces the free-energy barrier of nucleation for the acid-doped ASW samples.

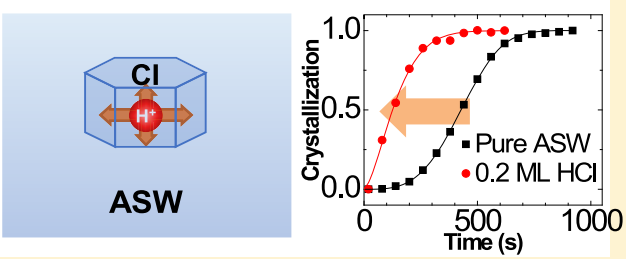

1. INTRODUCTION

The properties of amorphous solid water (ASW) have attracted considerable attention in recent years because of the structural resemblance of ASW to supercooled water as well as its astrophysical significance.[1−3] ASW films can be formed in the laboratory by condensation of water vapor onto a very cold substrate. Such ASW films are thermodynamically unstable and transform into crystalline ice (CI) at temperatures above ∼135 K on a laboratory time scale. The kinetics and mechanisms of this phase transition have been investigated by several researchers.[4−13] The apparent activation energy for crystallization of ASW samples has been observed to be in the range of 60−77 kJ·mol^{-1},[4,8−11] for which variations in the reported values may be related to the different rate-limiting steps in the investigated phenomena. Several researchers have studied the nucleation and growth steps of ASW crystallization separately by employing ingenious experimental schemes.[6,11] Dohnálek et al.[6] investigated the crystallization kinetics of thin ASW films deposited on a CI substrate and observed a dramatic acceleration of the crystallization rate at the ASW/CI interface, where only the growth step was required for crystallization to occur. Safarik and Mullins[11] decoupled the nucleation and growth kinetics by splitting the sample heating procedure into two isothermal stages, that is, the prenucleation stage at a high temperature and the subsequent growth stage at low temperatures. These studies indicated that the energy barrier of the growth step was 47−56 kJ·mol^{-1}, which is significantly lower than the apparent activation energy of crystallization, and the nucleation step requires a much higher activation energy of 140−168 kJ·mol^{-1} as the bottleneck of crystallization.

The effect of impurities on ASW crystallization has also been studied. Souda[14] reported that methanol incorporated in ASW films induced the nucleation of water and reduced the crystallization temperature. McClure et al.[15] showed that ASW films containing dilute amounts of nitric acid (HNO_3) crystallized more rapidly than pure ASW films. Additionally, HNO_3 significantly reduced fracture formation in the crystallizing ASW films, as evidenced from the uptake and desorption behaviors of the probe molecules ($CClF_2H$ and CCl_4). The promotion of ASW crystallization by HNO_3 is opposite to the effect of ordinary solutes in aqueous solutions, which suppress freezing of the solutions. The cause of this interesting acid-promotion effect, however, has not been studied in depth, especially with regard to the properties of acid species responsible for crystallization and its mechanism.

In the present work, we investigated the effect of externally added HCl on the crystallization of ASW films with temperature-programmed desorption (TPD) and reflection−absorption infrared spectroscopy (RAIRS) measurements. The

Received: August 13, 2018
Revised: September 27, 2018
Published: September 28, 2018

DOI: 10.1021/acs.jpcc.8b07858
J. Phys. Chem. C 2018, 122, 24164−24170

crystallization kinetics were investigated by conducting isothermal kinetic measurements at different temperatures and by changing the location of HCl in the samples. The study showed that excess protons released from HCl promoted the crystallization of ASW by facilitating the nucleation process. A plausible thermodynamic explanation has also been suggested for the proton-induced crystallization phenomena.

2. EXPERIMENTAL SECTION

The experiments were carried out in an ultrahigh vacuum (UHV) chamber equipped with a quadrupole mass spectrometer (Extrel, Model 5221), a low energy Cs^+ ion gun (Kimball Physics, ILG-4/IGPS-4), and a Fourier-transform infrared spectrometer (PerkinElmer, Spectrum 100).[16,17] TPD, RAIRS, low energy sputtering (LES), and reactive ion scattering (RIS) experiments were performed using these instruments.

A Pt(111) single crystal surface (Pt atom density = 1.5×10^{19} atoms·m^{-2}) was cleaned by Ar^+ ion sputtering at 2 keV daily and by heating at 1200 K three times before starting each experiment. ASW films were grown at 80 K on the cleaned Pt(111) surface by backfilling the chamber with water vapor at the partial pressure of $\sim 2 \times 10^{-7}$ Torr through a leak valve, unless specified otherwise. The thickness of the ASW films was typically set at 180 ML (1 ML = 1.1×10^{19} water molecules·m^{-2}). The film thickness was varied between 90 and 360 ML in thickness dependence studies. The film thickness was kept greater than the critical thickness (~50 ML) to avoid a roughening transition during crystallization on the Pt(111) surface.[18−20] Hydrogen chloride (HCl, Aldrich, ≥99% purity) gas was exposed onto the sample surface through a tube doser connected to a leak valve. During the procedure, the sample temperature was kept at 80 K unless otherwise specified, and the partial pressure of HCl inside the UHV chamber was maintained below 1×10^{-9} during gas exposure. NaCl was deposited onto the sample surface using a home-made thermal evaporator charged with NaCl powder. The evaporator was heated to 700 K for NaCl deposition, and the deposition time was controlled by a mechanical shutter installed in front of the evaporator.

TPD experiments were performed to monitor the crystallization temperature of the ASW films and to estimate the film thickness and amount of HCl in the samples. TPD intensity of HCl from the ASW film was calibrated against the TPD intensity of HCl adsorbed on a Pt(111) surface, which showed a well-discernible desorption feature at 150−400 K for 0.2 ML coverage.[21] The thickness of an ASW film was estimated from the ratio of the TPD intensity of the ASW film to that of water monolayer on Pt(111). The crystallization of the ASW sample was indicated by a bump in the TPD profile near 155 K, which appeared because of the reduction in the sublimation rate upon crystallization.[4,5,9]

RAIRS measurements were conducted in a grazing angle (84°) reflection geometry. IR light with p-polarization through a wire-grid polarizer (Edmund Optics) was reflected from the sample and entered an external mercury−cadmium−telluride detector. The beam path outside the UHV chamber was purged using high-purity N_2 gas to remove water vapor and carbon dioxide impurities. The spectra were averaged 256 times with a spectral resolution of 4 cm^{-1}.

3. RESULTS

3.1. Crystallization of ASW Films with HCl Adsorbates. As a prerequisite of investigating the effect of adsorbed HCl on the crystallization of ASW films, the chemical states of HCl on the ASW surface were examined by RIS, LES, and RAIRS. The results of these experiments (Section S1 of Supporting Information) showed that HCl was completely dissociated into H^+ and Cl^- ions upon adsorption onto or insertion into the ASW films at 80 K.[22]

The crystallization temperature of ASW films was monitored by TPD. As shown in Figure 1a, the TPD profile of a pure

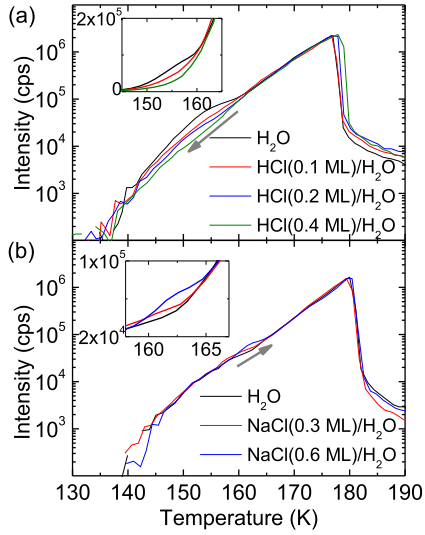

Figure 1. Water TPD spectra of (a) HCl and (b) NaCl-adsorbed H_2O−ASW (180 ML) films on a Pt(111) single crystal. The temperature ramp rate was 1 K·s^{-1} for all samples. Gray arrows are marked to emphasize the changes in the crystallization temperature with the increasing HCl or NaCl coverage. The insets in (a,b) show the desorption curves of corresponding samples on a linear intensity scale for visualizing the crystallization bumps with more clarity.

ASW film exhibited a bump structure near 155 K due to crystallization. This bump was more clearly visible in the linear intensity curve (inset of Figure 1a). When HCl was added onto the ASW film surface for 0.1 ML coverage, the bump shifted to a lower temperature. This behavior indicated that the HCl adsorbate accelerated the crystallization of the sample. With increasing coverage of HCl, the temperature of the bump shifted further downward and its height decreased. The bump became nearly invisible at HCl coverage of 0.4 ML, which indicated that the sample may have crystallized before the water desorption signal from the sample became strong (<140 K). In the study by McClure et al.,[15] similar changes in the water TPD signals were observed upon the addition of HNO_3 to ASW films.

To determine which of the H^+ and Cl^- ions are responsible for the acceleration of ASW crystallization, we examined the effect of NaCl adsorbates on the crystallization. NaCl was completely ionized on the ASW surface.[23] As shown in Figure 1b, the crystallization temperature of NaCl-added ASW films increased with increasing NaCl coverage. This showed that NaCl impeded the crystallization process. As Cl^- ions were commonly present on the surfaces of both HCl-adsorbed and NaCl-adsorbed samples, H^+ must be the cause of the accelerated crystallization of ASW.

DOI: 10.1021/acs.jpcc.8b07858
J. Phys. Chem. C 2018, 122, 24164−24170

RAIRS experiments monitored the progress of crystallization of ASW films under isothermal conditions. A pure or HCl-doped ASW film, prepared at 80 K, was heated to a fixed temperature between 137 and 145 K. Then, promptly RAIR spectra were recorded as a function of time for isothermal kinetic measurements at the corresponding temperature. The first recorded RAIR spectrum (the red curve in Figure 2a)

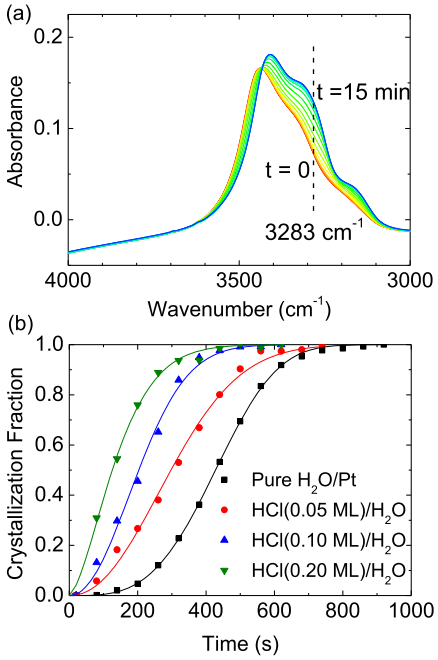

Figure 2. (a) Isothermal spectral change of the ν(O−H) stretch band of a pure ASW film at 143 K for 0−15 min. The dashed line marks the wavenumber (3283 cm^{-1}) that was used to estimate the crystallization fraction. (b) Crystallization fraction of pure and HCl-adsorbed H_2O−ASW (180 ML) films [HCl(0−0.2 ML)/H_2O(180 ML)/Pt(111)] obtained from isothermal RAIRS measurements at 143 K. Solid lines are the Avrami equations fitted to the experimental data. The fitting parameters are given in Table S1 (Supporting Information).

indicated an almost entirely amorphous nature of the sample. The spectral shape changed gradually in time and indicated complete crystallization of a sample with no further spectral change after 15 min (the blue curve in Figure 2a). The intermittent spectra represented the progress of crystallization and were deconvoluted as a linear combination of the ASW and CI spectra to deduce the crystallization fraction, $x(t)$, of a sample at time t. In practice, changes in the absorbance at a fixed wavenumber (3283 cm^{-1} in Figure 2a, indicated by dashed line) produced basically the same result for $x(t)$ as that obtained from the deconvolution of the spectral shape.

Figure 2b illustrates the changes in the crystallization fractions of pure and HCl-adsorbed ASW samples as measured from the isothermal kinetic experiments conducted at 143 K. In this case, the absolute magnitude of the absorbance difference between the ASW and CI films varied with the HCl content of the sample. Therefore, the absorbance difference was normalized to compensate this variation (Section S3, Supporting Information) in the plots shown in Figure 2b. It was evident that the speed of crystallization increased with the increasing HCl coverage. The crystallization fraction curves fitted well with the Avrami equation (eq 1),[24,25] which is shown by the solid lines in Figure 2b.

$$x(t) = 1 - \exp(-kt^n) \quad (1)$$

where k is a crystallization rate coefficient and n is the time exponent. The estimated values of k and n from the curve fitting are listed in Table S1 (Supporting Information). It should be noted that n decreased from 3.43 ± 0.05 to 1.52 ± 0.05 as HCl coverage increased from 0 to 0.2 ML. This change was reflected in the change of the curve shape from sigmoidal to exponential. In the case where crystallization initiates at random nucleation sites in the bulk and expands toward all directions, n = 4 for bulk samples and $n \approx 3$ for thin films.[26,27] On the other hand, in the case where nucleation occurs at the surface of ASW films, the direction of crystal growth is limited perpendicular to the surface,[27] and n becomes close to 1. For example, as reported by Smith et al.,[28] crystallization of an ASW film started at the ASW/CI interface with $n \approx 1.4$. In the present result, n = 3.43 for a pure ASW film is consistent with random nucleation in the bulk phase. On the other hand, the decrease in the value of n to 1.52 at 0.2 ML HCl coverage indicated that nucleation started preferentially at the surface of the HCl/ASW film, that is, where HCl was located.

Temperature dependence of the crystallization kinetics was examined for pure and HCl-adsorbed ASW films in the temperature region of 137−145 K. The results are displayed in Figure 3 with the fitting parameters summarized in Table S2

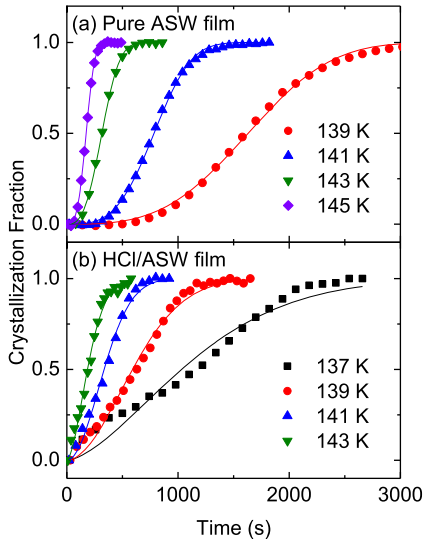

Figure 3. Isothermal RAIRS measurements of the crystallization fraction of (a) pure ASW film [H_2O(180 ML)/Pt(111)] and (b) HCl-adsorbed ASW film [HCl(0.1 ML)/H_2O(180 ML)/Pt(111)] at various temperatures. Solid lines are the Avrami equations fitted to the experimental data. The fitting parameters are given in Table S2 (Supporting Information). The discrepancy between the experimental and theoretical lines at 137 K in (b) could be related to interfering effects arising from the long measurement time (~45 min).

(Supporting Information). The crystallization rate increased at higher temperatures for all samples. When the crystallization rate was compared between pure and HCl-doped ASW films, it was evident that the addition of 0.1 ML HCl increased the crystallization rate about two-fold. The HCl adsorption also changed the sigmoidal curve shape of the graph of pure ASW samples to a nonsigmoidal shape. This change was reflected in the change of the fitting parameters. For example, n was 3.19 ± 0.07 for a pure ASW film at 139 K, which changed to 1.92 ± 0.08 for the HCl-doped film at the same temperature. As

DOI: 10.1021/acs.jpcc.8b07858
J. Phys. Chem. C 2018, 122, 24164−24170

mentioned above, the decrease in the value of n indicates the limited direction of growth as a result of reduced nucleation sites in the bulk phase.

The activation energy (E_a) of crystallization could be estimated from the temperature dependence of the crystallization curves. The crystallization half-time ($t_{1/2}$), defined as the time at which the crystallization fraction becomes 0.5, was inversely proportional to the crystallization rate and was used for the Arrhenius plots shown in Figure 4. The Arrhenius

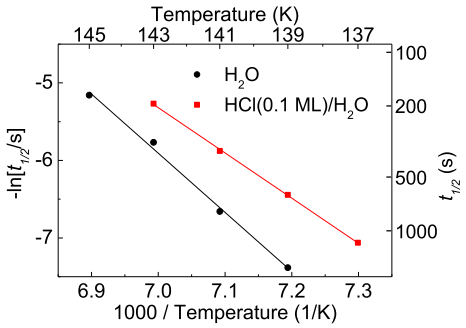

Figure 4. Arrhenius plot of the crystallization half-time ($t_{1/2}$) vs temperature estimated from the curves of Figure 3. Black circles and red squares are for the pure and 0.1 ML HCl-adsorbed ASW films, respectively. Solid lines are the Arrhenius fittings. The activation energies of crystallization are 63.4 ± 2.8 kJ·mol^{-1} for pure ASW films and 48.5 ± 0.6 kJ·mol^{-1} for HCl-adsorbed ASW films.

activation energy (E_a) for crystallization of pure ASW films was estimated to be 63.4 ± 2.8 kJ·mol^{-1}. This value is within the range of the previously reported values (60−77 kJ·mol^{-1}) obtained by different experimental measurements.[4,8−11] On the other hand, when 0.1 ML HCl was adsorbed on ASW films, E_a was reduced to 48.5 ± 0.6 kJ·mol^{-1}. Interestingly, this value is close to the activation energy for crystal growth from pure ASW films, 47−56 kJ·mol^{-1}.[6,11] The apparent activation energy of crystallization comprises the activation energies of the nucleation and growth steps. The decrease in E_a for HCl-doped samples close to that of the growth step implied that the growth step was the bottleneck in the crystallization of HCl-doped samples. Thus, it could be interpreted that the excess protons greatly reduced the activation energy of nucleation. This possibility is further examined in the following section.

3.2. Nucleation Sites. The nucleation sites for the crystallization of HCl/ASW samples were investigated by two different methods. In one approach, the dependence of crystallization kinetics on the film thickness was investigated. As demonstrated in the previous studies by Safarik et al.,[12,29] if nucleation occurs in bulk ASW, the crystallite grains grow larger in a thicker ASW film, which makes such films crystallize faster than thin films. On the other hand, if crystallization initiates at the surface of the ASW film, crystallization takes longer for a thicker film than a thinner film because the propagating distance of crystal growth is longer for the former. As shown in Figure 5, the HCl/ASW film with 90 ML thickness crystallized faster than those with 180 and 360 ML thicknesses. This result indicated that crystallization started at the vacuum/ASW interface, where the acid molecules were located, rather than in the bulk phase. On the other hand, previous studies suggest that a thicker pure ASW film crystallizes faster because of bulk nucleation.[12] We excluded the possibility that the ASW/Pt interface of the present samples is the nucleation site. This is because pure and HCl-

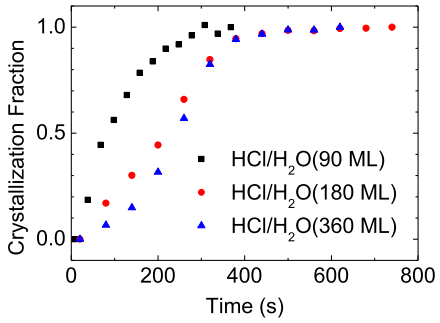

Figure 5. Isothermal measurement of the crystallization fraction of 0.1 ML HCl-adsorbed ASW films monitored by RAIRS at 143 K. The thicknesses of the ASW films are 90, 180, and 360 ML.

adsorbed ASW samples showed opposite thickness dependences for the crystallization rate, contrary to the behavior expected from the common existence of the ASW/Pt interface in both of them.

In the other approach, we placed the HDO probe species at different specific positions of the HCl-adsorbed ASW films, as depicted in Figure 6a, and monitored the crystallization fraction at these positions from the shifts in the O−D stretching frequency of HDO as a function of crystallization time (the so-called "selective placement" method[7,8]). A liquid mixture of 5% D_2O and 95% H_2O was prepared, which produced 90% H_2O, 10% HDO, and a minute amount of D_2O as a result of rapid H/D exchange at room temperature. The vapor of this liquid mixture was exposed to a sample surface to construct various stacking structures containing an HDO layer in the HCl/H_2O−ASW film. In these samples, the ν(O−D) band intensity originated mostly from the O−D stretch of HDO that was vibrationally isolated from bulk H_2O vibrations, while the contributions of symmetric and asymmetric O−D stretch intensities of D_2O were relatively insignificant. Crystallization of the samples shifted the ν(O−D) frequency to a lower wavenumber and narrowed the band width, as shown in Figure 6b. Consequently, monitoring the changes in this band, originating from HDO inserted at different locations of the HCl/H_2O−ASW films, provided information about crystal growth through the films. Figure 6c shows the changes in the crystallization fraction of the HDO species embedded at different locations in the samples. It shows that the HDO species closer to the film surface crystallized earlier. On the other hand, in Figure 6d, the crystallization fraction estimated from the bulk ν(O−H) signals (originating from H_2O and HDO) indicated that the bulk crystallization rate ($t_{1/2} \approx 190$ s) was independent of the location of HDO in the samples. These results clearly indicated that nucleation occurred at the vacuum/ASW interface, where HCl was added, and crystallization propagated through the film interior. The two different experimental measurements consistently support this crystallization behavior.

We placed HCl at different locations in the ASW films and measured their crystallization rate to explore the relationship between the location of the nucleation sites and the speed of crystallization. We may consider that added HCl is localized in the samples because H^+ ions reside close to the location of HCl injection with the average spread distance of several molecular layers in ASW at low temperatures,[30,31] despite its mobility. Figure 7 displays the half-time of crystallization versus the depth of HCl from the ASW surface. Crystallization

DOI: 10.1021/acs.jpcc.8b07858
J. Phys. Chem. C 2018, 122, 24164−24170

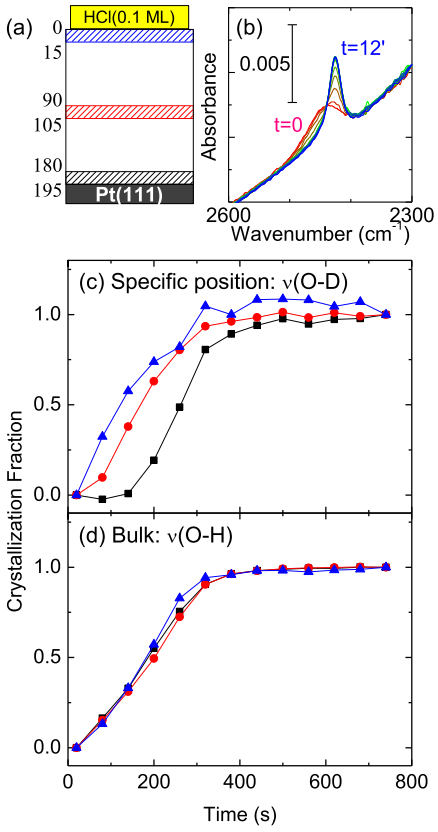

Figure 6. Isothermal RAIRS measurements of the crystallization fraction of 0.1 ML HCl-adsorbed ASW films at 143 K. (a) Structure of the HCl/H_2O−ASW samples, which indicates three different locations of the HDO probe molecules (indicated by colored hatch patterns) in the samples. An HDO layer (95% H_2O + 5% D_2O, 15 ML thickness) was placed at the vacuum/ASW interface (black squares), in the middle of ASW film (red circles), and at the ASW H_2O/Pt(111) interface (blue triangles). The thickness of the H_2O−ASW film was 180 ML, which implied that the total sample thickness was 195 ML. (b) Changes in the ν(O−D) stretching band of HDO with crystallization time (0−12 min) shown for the sample with the HDO layer in the middle. The red curve was the first recorded spectrum at t = 0 and indicated almost entirely ASW, whereas the blue curve was the spectrum at t = 12 min and indicated almost entirely CI. (c) Crystallization fraction as a function of time, measured at the location of the HDO layer for three samples by monitoring the changes in the ν(O−D) band (2425 cm^{-1}) intensity. (d) Crystallization fraction of the entire sample measured from the changes in the ν(O−H) band (~3283 cm^{-1}) intensities of H_2O and HDO.

occurred fastest when HCl was placed in the middle of the film (HCl-center). When the location of HCl was moved away from the center, crystallization took longer. Relative to the HCl/ASW/Pt sample (HCl-on-top), the crystallization half-time of the HCl-center sample (the red circle in Figure 7) was reduced to about half. This observation was also supported by nucleation near the location of HCl injection. For the HCl-center sample, crystals could grow in both directions (toward both interfaces) from the center. On the other hand, for the HCl/ASW/Pt sample, the growth could occur only in one direction and its propagation across the whole film thickness took nearly twice as long.

The crystallization speed of the ASW/HCl/Pt sample (the blue circle in Figure 7) was almost as slow as that of the pure ASW samples. This suggested that the excess protons at the

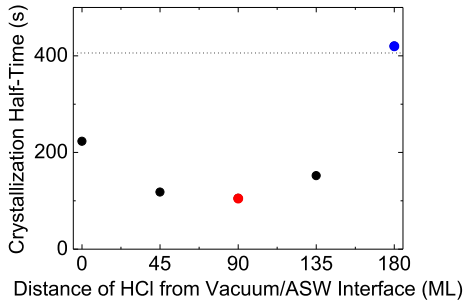

Figure 7. Crystallization half-time ($t_{1/2}$) vs the depth of HCl from the ASW surface. The amount of added HCl was 0.1 ML, and the thickness of the H_2O ASW film was 180 ML. The crystallization rate was measured at 143 K. The dotted line indicates $t_{1/2}$ of a pure ASW film. The red solid circle corresponds to the sample with HCl in the middle, and the blue solid circle corresponds to the sample with HCl at the ASW/Pt interface.

ASW/Pt interface are not an effective nucleation promotor. It has been reported[32] that protons at the ASW/Pt interface can be stabilized by forming multiply hydrated proton structures. Therefore, the stable protons trapped at the interface may not be able to participate in the formation of crystallites in the interfacial ASW layer.

4. DISCUSSION

The experimental observations (Section 3) showed that excess protons promote the crystallization of ASW samples by assisting nucleation near the place where the acids are injected. Then, an interesting question is the mechanism by which the excess protons assist in the formation of crystalline nuclei in ASW. It is well known that acid impurities increase proton mobility in ice, resulting in protonic isotope mixing[33−35] as well as hydrogen-bond polarization in the ice lattice.[36] However, crystallization of ASW requires a movement of both oxygen atoms and protons. Therefore, a key question is how oxygen or an entire water molecule can be moved with the help of excess protons. Experimental evidence suggests that ions (ionized acids, bases, and salts) can affect the viscosity and hydrogen-bonding network of liquid water.[37] In analogy, it may be expected that ionized acids affect the corresponding properties of ASW, which may somehow alter the crystallization behavior. However, a detailed molecular mechanism by which acids act on water crystallization is difficult to contemplate at the present stage because of the lack of understanding of ion−water interaction and its relation to the crystallization phenomena. According to recent molecular dynamics simulations of water molecules penetrating into a carbon nanotube, the excess proton in the water system creates its own transport pathway into the nanotube by assisting in the formation of a water wire.[38] This example illustrates that the excess protons can alter the hydrogen-bonding configuration of nearby water molecules to facilitate proton migration. Other similar molecular pathways by which proton dynamics may assist the formation of an ordered H-bonding structure in a localized region can be imagined. However, the present result does not provide explicit evidence about the molecular mechanism of nuclei formation in ASW, and answer to this question may be left for future study.

We propose a plausible thermodynamic explanation for the proton-induced crystallization of ASW. Recent studies[39,40] have shown that excess protons released from an acid into ice

DOI: 10.1021/acs.jpcc.8b07858
J. Phys. Chem. C 2018, 122, 24164−24170

greatly increased the configurational entropy, $\Delta S_{conf} = k \ln W$, where W is the number of accessible positions in the lattice by excess protons. ΔS_{conf} originates from the high mobility of the protons in ice via the Grotthuss shuttling mechanism[41,42] and has been estimated to be as large as ~60 J mol^{-1} K^{-1} in ASW films grown at 70−80 K.[40] It has also been shown that this proton entropy can significantly enhance proton transfer reactions in ASW even at low temperatures (8−140 K), including the dissociation of weak acids.[40] In the case of ASW crystallization investigated in the present study, ΔS_{conf} may contribute to reducing the free-energy barrier of nucleation. This is because ΔS_{conf} of excess protons is larger in CI with an ordered structure, where the proton transport distance is longer, as compared to ASW, where the proton transport distance is limited as a result of abundant trapping sites. For this reason, ΔS_{conf} of excess protons increases upon nucleation in ASW, and this lowers the free energy barrier of the nucleation. Consider the formation of crystallizing nuclei composed of, for instance, 10 water molecules in the vicinity of an excess proton. Upon the nucleation, the excess proton becomes mobile over 10 water molecules, and each water molecule has two possible sites to accept an excess proton ($W = 10 \times 2$). The resultant increase in ΔS_{conf} will reduce the free energy of the nucleation by $\Delta G = -T\Delta S_{conf} \approx -4$ kJ·mol^{-1} at 150 K, if we assume that the excess proton was initially trapped at defect sites ($W \approx 1$) before nucleation. Although this is a very crude estimation, it serves to qualitatively demonstrate that ΔS_{conf} can significantly lower the free energy of nucleation. For comparison, the free energy of bulk CI is lower than that of ASW by only 1−2 kJ·mol^{-1} for pure water.[4,9,43] Therefore, the additional effect of ΔS_{conf} can significantly reduce the free energy of nucleation for acid-doped ASW, although this effect does not significantly change the bulk-state free energy due to dilute concentration of excess protons in the sample. According to a classical nucleation theory, the activation energy of nucleus formation is inversely proportional to the square of the free energy difference between the two bulk phases.[26,27] For this reason, the protonic entropy effect could appear amplified in lowering the nucleation barrier height as compared to the lowering of the free energy of the bulk states.

The acid-promoted crystallization of ASW may be an interesting but unusual example that entropy drives a phase transition from a disordered to ordered state. This phenomenon might appear contradictory to the general behavior that a crystallizing phase transition reduces the entropy of the system. However, in the present system, only the entropy of the excess protons is increased by crystallization. Other thermodynamic values related to ASW crystallization, including the usual negative entropic change associated with the formation of an ordered H-bonding network, may not significantly differ from the case of crystallization of pure ASW samples.

The effect of configurational entropy of excess protons may also exist for ASW crystallization in the presence of other acids, including the observation that HNO_3 accelerates the crystallization of ASW films with reduced fracture formation in the samples.[15] Also, recent optical microscopy studies of crystal growth on ice crystal surfaces have shown that ice crystals grow preferentially from water droplet surfaces containing HCl,[44] which may suggest the existence of the acid-promotion effect for crystal growth at the water/ice interface.

5. CONCLUSIONS

The study of crystallization of HCl-doped ASW films with TPD and RAIRS measurements showed that the excess protons promoted the crystallization of the ASW films. In contrast, Na^+ ions had the opposite effect and hindered the crystallization process, similar to the freezing point depression of aqueous solutions with ordinary electrolyte ions. The temperature dependence study of crystallization rates showed that excess protons lowered the overall activation energy of crystallization to a value close to the activation energy of crystal growth. This suggested that the kinetic bottleneck of crystallization changed from nucleation to crystal growth in the presence of excess protons. The study of nucleation sites in the samples showed that crystallization started near the location of proton injection, regardless of whether it was the vacuum/ASW interface or the film interior. These observations altogether indicated that the excess protons facilitated the formation of crystallizing nuclei and thus accelerated the crystallization process. We have proposed an explanation based on thermodynamics that the increased configurational entropy of the excess protons in ice likely lowers the free-energy barrier of nucleation for the acid-doped ASW samples relative to that for the pure ASW samples.

■ ASSOCIATED CONTENT

Supporting Information

The Supporting Information is available free of charge on the ACS Publications website at DOI: 10.1021/acs.jpcc.8b07858.

Ionic dissociation of HCl on the ASW surface; fitting parameters of Avrami equation for Figures 2 and 3; and spectral changes of ν(O−H) band for HCl-adsorbed ASW films during crystallization (PDF)

■ AUTHOR INFORMATION

Corresponding Author

*E-mail: surfion@snu.ac.kr. Phone: +82 2 875 7471. Fax: +82 2 889 8156.

ORCID

Heon Kang: 0000-0002-7530-4100

Notes

The authors declare no competing financial interest.

■ ACKNOWLEDGMENTS

This work was supported by Samsung Science and Technology Foundation (SSTF-BA1301-04).

■ REFERENCES

(1) Angell, C. A. Amorphous Water. *Annu. Rev. Phys. Chem.* **2004**, *55*, 559−583.

(2) Smith, R. S.; Petrik, N. G.; Kimmel, G. A.; Kay, B. D. Thermal and Nonthermal Physiochemical Processes in Nanoscale Films of Amorphous Solid Water. *Acc. Chem. Res.* **2012**, *45*, 33−42.

(3) Jenniskens, P.; Blake, D. Structural Transitions in Amorphous Water Ice and Astrophysical Implications. *Science* **1994**, *265*, 753−756.

(4) Löfgren, P.; Ahlström, P.; Lausma, J.; Kasemo, B.; Chakarov, D. Crystallization Kinetics of Thin Amorphous Water Films on Surfaces. *Langmuir* **2003**, *19*, 265−274.

(5) Smith, R. S.; Huang, C.; Wong, E. K. L.; Kay, B. D. Desorption and Crystallization Kinetics in Nanoscale Thin Films of Amorphous Water Ice. *Surf. Sci.* **1996**, *367*, L13−L18.

DOI: 10.1021/acs.jpcc.8b07858
J. Phys. Chem. C 2018, 122, 24164−24170

(6) Dohnálek, Z.; Kimmel, G. A.; Ciolli, R. L.; Stevenson, K. P.; Smith, R. S.; Kay, B. D. The Effect of the Underlying Substrate on the Crystallization Kinetics of Dense Amorphous Solid Water Films. *J. Chem. Phys.* **2000**, *112*, 5932−5941.
(7) Yuan, C.; Smith, R. S.; Kay, B. D. Surface and Bulk Crystallization of Amorphous Solid Water Films: Confirmation of "Top-Down" Crystallization. *Surf. Sci.* **2016**, *652*, 350−354.
(8) Yuan, C.; Smith, R. S.; Kay, B. D. Communication: Distinguishing between Bulk and Interface-Enhanced Crystallization in Nanoscale Films of Amorphous Solid Water. *J. Chem. Phys.* **2017**, *146*, 031102.
(9) Smith, R. S.; Matthiesen, J.; Knox, J.; Kay, B. D. Crystallization Kinetics and Excess Free Energy of H_2O and D_2O Nanoscale Films of Amorphous Solid Water. *J. Phys. Chem. A* **2011**, *115*, 5908−5917.
(10) Kondo, T.; Kato, H. S.; Bonn, M.; Kawai, M. Deposition and Crystallization Studies of Thin Amorphous Solid Water Films on Ru(0001) and on CO-Precovered Ru(0001). *J. Chem. Phys.* **2007**, *127*, 094703.
(11) Safarik, D. J.; Mullins, C. B. The Nucleation Rate of Crystalline Ice in Amorphous Solid Water. *J. Chem. Phys.* **2004**, *121*, 6003−6010.
(12) Safarik, D. J.; Meyer, R. J.; Mullins, C. B. Thickness Dependent Crystallization Kinetics of Sub-Micron Amorphous Solid Water Films. *J. Chem. Phys.* **2003**, *118*, 4660−4671.
(13) Backus, E. H. G.; Grecea, M. L.; Kleyn, A. W.; Bonn, M. Surface Crystallization of Amorphous Solid Water. *Phys. Rev. Lett.* **2004**, *92*, 236101.
(14) Souda, R. Effects of Methanol on Crystallization of Water in the Deeply Supercooled Region. *Phys. Rev. B: Condens. Matter Mater. Phys.* **2007**, *75*, 184116.
(15) McClure, S. M.; Barlow, E. T.; Akin, M. C.; Tanaka, P. L.; Safarik, D. J.; Truskett, T. M.; Mullins, C. B. Effect of Dilute Nitric Acid on Crystallization and Fracture of Amorphous Solid Water Films. *J. Phys. Chem. C* **2007**, *111*, 10438−10447.
(16) Kang, H. Chemistry of Ice Surfaces. Elementary Reaction Steps on Ice Studied by Reactive Ion Scattering. *Acc. Chem. Res.* **2005**, *38*, 893−900.
(17) Kang, H. Reactive Ion Scattering of Low Energy Cs^+ from Surfaces. A Technique for Surface Molecular Analysis. *Bull. Korean Chem. Soc.* **2011**, *32*, 389−398.
(18) Hodgson, A.; Haq, S. Water Adsorption and the Wetting of Metal Surfaces. *Surf. Sci. Rep.* **2009**, *64*, 381−451.
(19) Thürmer, K.; Bartelt, N. C. Nucleation-Limited Dewetting of Ice Films on Pt(111). *Phys. Rev. Lett.* **2008**, *100*, 186101.
(20) Thürmer, K.; Bartelt, N. C. Growth of Multilayer Ice Films and the Formation of Cubic Ice Imaged with STM. *Phys. Rev. B: Condens. Matter Mater. Phys.* **2008**, *77*, 195425.
(21) Daschbach, J. L.; Kim, J.; Ayotte, P.; Smith, R. S.; Kay, B. D. Adsorption and Desorption of HCl on Pt(111). *J. Phys. Chem. B* **2005**, *109*, 15506−15514.
(22) Park, S.-C.; Kang, H. Adsorption, Ionization, and Migration of Hydrogen Chloride on Ice Films at Temperatures between 100 and 140 K. *J. Phys. Chem. B* **2005**, *109*, 5124−5132.
(23) Park, S.-C.; Pradeep, T.; Kang, H. Ionic Dissociation at NaCl on Frozen Water. *J. Chem. Phys.* **2000**, *113*, 9373−9376.
(24) Avrami, M. Kinetics of Phase Change. I General Theory. *J. Chem. Phys.* **1939**, *7*, 1103−1112.
(25) Avrami, M. Kinetics of Phase Change. II Transformation-Time Relations for Random Distribution of Nuclei. *J. Chem. Phys.* **1940**, *8*, 212−224.
(26) Rao, C. N. R.; Rao, K. J. *Phase Transitions in Solids: An Approach to the Study of the Chemistry and Physics of Solids*; McGraw-Hill: New York, 1978; pp 81−173.
(27) Jena, A. K.; Chaturvedi, M. C. *Phase Transformation in Materials*; Prentice Hall: Englewood Cliffs, NJ, 1992.
(28) Smith, R. S.; Dohnálek, Z.; Kimmel, G. A.; Teeter, G.; Ayotte, P.; Daschbach, J. L.; Kay, B. D. *Water in Confining Geometries*; Buch, V., Devlin, J. P., Eds.; Springer: Berlin Heidelberg, 2003; pp 337−357.
(29) Safarik, D. J.; Mullins, C. B. Surface Phase Transformation Kinetics: A Geometrical Model for Thin Films of Nonvolatile and Volatile Solids. *J. Chem. Phys.* **2002**, *117*, 8110−8123.
(30) Park, E.; Lee, D. H.; Kim, S.; Kang, H. Transport and Surface Accumulation of Hydroniums and Chlorides in an Ice Film. A High Temperature (140−180 K) Study. *J. Phys. Chem. C* **2012**, *116*, 21828−21835.
(31) Lee, D. H.; Bang, J.; Kang, H. Surface Charge Layer of Amorphous Solid Water with Adsorbed Acid or Base: Asymmetric Depth Distributions of H^+ and OH^- Ions. *J. Phys. Chem. C* **2016**, *120*, 12051−12058.
(32) Kim, Y.; Noh, C.; Jung, Y.; Kang, H. The Nature of Hydrated Protons on Platinum Surfaces. *Chem.—Eur. J.* **2017**, *23*, 17566−17575.
(33) Collier, W. B.; Ritzhaupt, G.; Devlin, J. P. Spectroscopically Evaluated Rates and Energies for Proton-Transfer and Bjerrum Defect Migration in Cubic Ice. *J. Phys. Chem.* **1984**, *88*, 363−368.
(34) Devlin, J. P.; Buch, V. Evidence for the Surface Origin of Point Defects in Ice: Control of Interior Proton Activity by Adsorbates. *J. Chem. Phys.* **2007**, *127*, 091101.
(35) Moon, E.-S.; Yoon, J.; Kang, H. Energy Barrier of Proton Transfer at Ice Surfaces. *J. Chem. Phys.* **2010**, *133*, 044709.
(36) Ueda, M.; Matsuo, T.; Suga, H. Calorimetric Study of Proton Ordering in Hexagonal Ice Catalyzed by Hydrogen Fluoride. *J. Phys. Chem. Solids* **1982**, *43*, 1165−1172.
(37) Marcus, Y. *Ion Solvation*; John Wiley and Sons Ltd: Chichester, U.K., 1985.
(38) Peng, Y.; Swanson, J. M. J.; Kang, S.-g.; Zhou, R.; Voth, G. A. Hydrated Excess Protons Can Create Their Own Water Wires. *J. Phys. Chem. B* **2015**, *119*, 9212−9218.
(39) Shin, S.; Park, Y.; Kim, Y.; Kang, H. Dissociation of Trifluoroacetic Acid in Amorphous Solid Water: Charge-Delocalized Hydroniums and Zundel Continuum Absorption. *J. Phys. Chem. C* **2017**, *121*, 12842−12848.
(40) Park, Y.; Shin, S.; Kang, H. Entropy-Driven Spontaneous Reaction in Cryogenic Ice: Dissociation of Fluoroacetic Acids. *J. Phys. Chem. Lett.* **2018**, *9*, 4282−4286.
(41) Eigen, M.; de Maeyer, L. Self-Dissociation and Protonic Charge Transport in Water and Ice. *Proc. R. Soc. London, Ser. A* **1958**, *247*, 505−533.
(42) Kobayashi, C.; Saito, S.; Ohmine, I. Mechanism of Fast Proton Transfer in Ice: Potential Energy Surface and Reaction Coordinate Analyses. *J. Chem. Phys.* **2000**, *113*, 9090−9100.
(43) Ahlström, P.; Löfgren, P.; Lausma, J.; Kasemo, B.; Chakarov, D. Crystallization Kinetics of Thin Amorphous Water Films on Surfaces: Theory and Computer Modeling. *Phys. Chem. Chem. Phys.* **2004**, *6*, 1890−1898.
(44) Nagashima, K.; Sazaki, G.; Hama, T.; Murata, K.-i.; Furukawa, Y. Uptake Mechanism of Atmospheric Hydrogen Chloride Gas in Ice Crystals Via Hydrochloric Acid Droplets. *Cryst. Growth Des.* **2018**, *18*, 4117−4122.

DOI: 10.1021/acs.jpcc.8b07858
J. Phys. Chem. C 2018, 122, 24164−24170